Observational black hole spectroscopy: A time-domain multimode analysis of GW150914

Gregorio Carullo, Walter Del Pozzo, and John Veitch

Observational Black Hole Spectroscopy:
A time-domain multimode analysis of GW150914

Gregorio Carullo,[1, 2] Walter Del Pozzo,[1, 2] and John Veitch[3]

[1]*Dipartimento di Fisica "Enrico Fermi", Università di Pisa, Pisa I-56127, Italy*
[2]*INFN sezione di Pisa, Pisa I-56127, Italy*
[3]*Institute for Gravitational Research, University of Glasgow, Glasgow, G12 8QQ, United Kingdom*

The detection of the least damped quasi-normal mode from the remnant of the gravitational wave event GW150914 realised the long sought possibility to observationally study the properties of quasi-stationary black hole spacetimes through gravitational waves. Past literature has extensively explored this possibility and the emerging field has been named "black hole spectroscopy". In this study, we present results regarding the ringdown spectrum of GW150914, obtained by application of Bayesian inference to identify and characterise the ringdown modes. We employ a pure time-domain analysis method which infers from the data the time of transition between the non-linear and quasi-linear regime of the post-merger emission in concert with all other parameters characterising the source. We find that the data provides no evidence for the presence of more than one quasi-normal mode. However, from the central frequency and damping time posteriors alone, no unambiguous identification of a single mode is possible. More in-depth analysis adopting a ringdown model based on results in perturbation theory over the Kerr metric, confirms that the data do not provide enough evidence to discriminate among an $l = 2$ and the $l = 3$ subset of modes. Our work provides the first comprehensive agnostic framework to observationally investigate astrophysical black holes' ringdown spectra.

INTRODUCTION

GW150914 [1], the loudest binary black hole (BBH) detected so far, provided evidence for the presence of a ringdown at the end of the coalescence. The ringdown spectrum, a superposition of quasi-normal modes (QNMs) and late-time power-law tails [2–5], directly ties to fundamental properties of the underlying spacetime. Due to the final state conjecture (i.e. no-hair theorems plus the conjecture that the Kerr solution is a dynamical attractor for BH spacetimes in astrophysical scenarios) [6–15] the physical spectrum of QNMs is exclusively determined by the asymptotic black hole (BH) mass and spin, hence ringdown observations of astrophysical BHs have the potential of verifying the Kerr nature of these objects. Moreover, an accurate determination of the BH ringdown spectrum represents one of the most promising avenues to unveil BH horizon quantum effects, discovering exotic compact objects, hairy BHs or even wormholes [16–18]. Several authors proposed methods and offered predictions on the feasibility of what has come to be known as "black hole spectroscopy" [19–21]. The improvements gained by coherently combining information from multiple events have also been investigated, see e.g. Ref. [22].

The first determination of a compact object QNM [23] by the LIGO and Virgo Collaborations (LVC) [24–26] revealed the intrinsic difficulties in determining the transition between the non-linear merger regime to the quasi-linear one, where the results of BH perturbation theory are applicable. Several studies based on numerical relativity simulations [27, 28], have proposed a start time of $\sim 15\,\mathrm{M}$ – M being the remnant mass – after the peak strain of the waveform (for an alternative approach see Ref. [29]). However, to validate these claims and to perform theory-agnostic measurements of the BH spectrum, we require the ability to measure the start time from the data. With this, we can robustly test the remarkable predictions of GR, such as the black hole area increase law [29].

In this paper, we present the first comprehensive spectroscopic analysis of the GW150914 ringdown signal that, by operating directly in time domain, successfully identifies from the data the time of transition as well as the most probable subset of QNMs in the data. This is achieved employing a generic damped sinusoids ringdown model which does not include GR predictions for its complex frequencies, hence generic enough to incorporate the emission of alternative compact objects possibly mimicking ringdown signals. We find no evidence in support of the presence of a second mode in addition to the one already identified in the LVC analysis. The central frequency and damping time measured with the generic model indicate that the most-probable modes can be identified with a subset of the the $\ell = 2$ and $\ell = 3$ modes as predicted by a Kerr solution [30]. We refine our results by adopting a model based on the theoretical spectrum of a Kerr BH. We demonstrate, in agreement with the generic approach, that the $(\ell, m, n) = (3, -3, 0), (3, -2, 0), (2, 1, 0)$ and $(2, 2, 0)$ modes are consistent with the remnant mass and spin of GW150914. The inferred transition time is consistent with the result obtained with the previous model. Unless explicitly noted, all statistical bounds reported are 90% credible regions.

TIME DOMAIN ANALYSIS

We perform our analysis in the time domain and use data from the Advanced LIGO detectors, provided by the Gravitational-Wave Open Science Center[31, 32]. We model the detector noise as a wide-sense stationary Gaussian process. We verify the validity of this assumption, confirming its validity, in agreement with the results published by the LVC collaboration at the time of the discovery, see e.g. Ref. [23]. The stochastic process describing the detector noise is thus fully described by its two-point autocovariance function $C(\tau)$:

$$C(\tau) = \int dt\, n(t)\, n(t+\tau)\,, \qquad (1)$$

which we estimate from 4096 s of data surrounding the event. The 4096 s of data sampled at a rate of 4096

Hz are band-passed with a 4th order Butterworth filter in the band [20,2028] Hz, then split into $\mathcal{X}$ second long chunks. The autocovariance is computed as the mean of the individual autocovariances estimated on each chunk, excluding the one containing the time of the trigger. To validate our noise estimation method, we exploit the Wiener-Khinchin theorem and compare the Discrete Fourier Transform (DFT) of the autocovariance with the power spectral density (PSD) computed with the standard Welch method. We find good agreement between the two estimates by choosing $\mathcal{X} = 2$. Any choice of $\mathcal{X} > 2$ does not affect our conclusions. The log-likelihood function for the observed strain series $d(t)$, given the presence of a GW signal $h(t)$ is:

$$\log p(d|\theta, I) = -\frac{1}{2} \int \int dt\, d\tau\, (d(t) - h(t; \theta))\, C^{-1}(\tau)\, (d(t+\tau) - h(t+\tau; \theta)),$$

where the domain of integration extends over the considered segment of data. The time-domain likelihood solves several technical issues of the analysis, providing a convenient framework to avoid Gibbs phenomena arising from the DFT of a fast-rising template which can pollute the analysis of the BH spectrum. The analysis was performed using a nested sampling algorithm [33].

AGNOSTIC ANALYSIS

We first perform an *agnostic* analysis of the GW150914 ringdown signal, without assuming GR predictions on the spectrum and intensity of the emission. Hence we relax as many assumptions as possible and assume a model defined by a superposition of damped sinusoids:

$$h_+ - i h_\times = \sum_n \mathcal{A}_n\, e^{i\tilde{\omega}_n(t - t_n) + \phi_n}\,. \qquad (2)$$

where $\tilde{\omega}_n \equiv \omega_n + i/\tau_n$ is the complex ringdown frequency. The parameters $\{\omega_n, \tau_n, \phi_n, \mathcal{A}_n, t_n\}_{n \in \mathcal{N}}$ are estimated directly from the data. The index n labels the $\mathcal{N}$ modes considered. Note that, in addition to the frequencies ω_n and damping times τ_n, we also infer the amplitudes $\mathcal{A}_n$ and start times t_n from the data.

The prior distribution on the intrinsic parameters was chosen to be uniform within the ranges: $f_n \in [100, 500]$ Hz, $\tau_n \in [0.5, 20]$ ms, $\log_{10} A_n \in [-23, -19]$, $\varphi_n \in [0, 2\pi]$ rad, $t_n \in [3.3, 6.6]$ ms after the peak of the waveform. The prior on the start time corresponds to the specific choice

of $[10, 20]\, M_f$ after the peak time of the strain (during the analysis $t = 1126259462.423$ s at LIGO Hanford site was chosen, in agreement with Ref. [23]). This choice is guided by numerical relativity studies that looked at the beginning of the linearized ringdown regime validity [34]. Different choices on the prior on the start time are presented in the *Discussion* section. $M_f = 68\, M_\odot$ (in geometric units) is the median value of the estimate presented in [35]. In addition to the intrinsic model parameters, we sample the sky position angles and polarisation, to obtain the detector strain:

$$h(t) = F_+(\alpha, \delta, \psi)\, h_+ + F_\times(\alpha, \delta, \psi)\, h_\times \qquad (3)$$

where $F_+(\alpha, \delta, \psi), F_\times(\alpha, \delta, \psi)$ are the detector angular response functions [36]. For all the models employed in this paper, we chose our prior distribution to be isotropic for the source's sky location, and uniform in the polarisation angle $\psi \in [0, \pi]$.

We begin by assuming a single mode damped sinusoid model to detect the most excited mode directly from the data. Fig. 3 shows the joint posterior distribution for the central frequency f and damping time τ from our analysis. We find $f = 234^{+11}_{-12}$ Hz and $\tau = 4.0^{+1.5}_{-1.0}$ ms, which is consistent both with the predicted values from a full Inspiral-Merger-Ringdown (IMR) analysis and with the late time ($t_{start} \geq t_{merger} + 3$ ms) unmodelled analyses in Refs. [21, 23]. To investigate which mode has the highest probability of matching the recovered unmodelled posterior *a posteriori*, according to GR predictions, we use the samples for the progenitors masses and spins
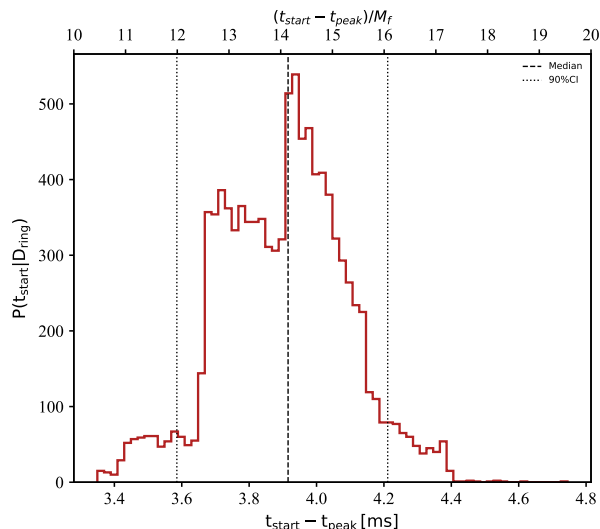
FIG. 1. Posterior distribution over $t_{\rm start}$ obtained assuming a uniform prior distribution in $[10, 20]\,M_f$.
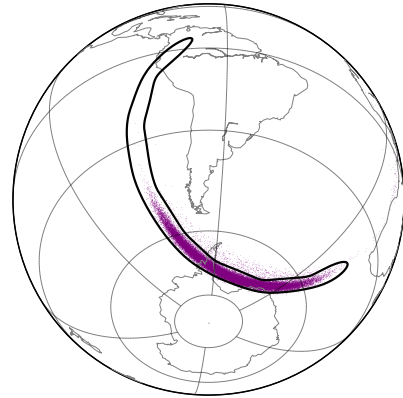

FIG. 2. Orthographic projection of the 90% two-dimensional contour for the sky position of GW150914 obtained by our analysis (in black). As a comparison we also show the publicly available posterior samples from a full IMR analysis by the LVC [37] (in purple, completely overlapping with our result). Regardless of the particular model chosen for the analysis, we always observe the same posterior.

released by the LVC [37], combined with fitting formulae obtained from numerical relativity simulations [20, 38, 39] and employ them to *predict* the corresponding frequency and damping time for a set of modes which overlap with the unmodelled posterior. Figure 3 shows the 90% CI on $n = 0$, $l = 2, 3$ modes obtained with the described procedure. The largest overlap, quantified through Bayes' theorem, is obtained for the $\{(2, 2, 0), (3, -3, 0)\}$ modes. We also find $\mathcal{A} = (3.22^{+1.4}_{-1.1}) \times 10^{-21}$, and, most notably, we determine, directly from the data, $t_{\rm start} = 3.9^{+0.3}_{-0.3}$ ms, Fig. 1.

The uncertainty on $t_{\rm start}$ is mostly due to the 4096 Hz sampling rate used. Interestingly, with a BH mass of $M_f = 68\,M_\odot$ (the median value published by the LVC [23]), one obtains a start time for the ringdown of $\sim 14^{+2}_{-2}\,M_f$. This result is in good agreement with what obtained through gauge-invariant geometric and algebraic conditions quantifying local isometry to the Kerr space-time [27] and results obtained through earlier parameter estimation methods [28]. We also infer a posterior distribution on the sky position of the signal, Fig 2, which completely overlaps with published LVC analyses using the full signal [37, 40]. The projection was obtained using a Dirichlet Process Gaussian-mixture model, as described in [41]. Due to the lower SNR contained in the ringdown-only portion of the signal, our posterior distribution is wider. Also, we observe no correlation between $t_{\rm start}$ and sky position parameters. Fig. 4 shows the reconstructed signal overlaid on interferometric data. A whitening procedure is applied in order to facilitate the visualization of the result, but no whitening is applied during the analysis.

At this point it is natural to ask whether the data provides evidence for a second ringdown mode. To verify this hypothesis we repeat the previous analysis using the

aforementioned settings, but now using two independent damped sinusoids. The Bayes' factor, see Table I, shows no evidence for more than a single mode. We also attempted a test of GR through the measurement of $\delta\omega$ following [42], but the posterior was uninformative, because the SNR is not enough to constrain more than a single mode. Finally, a preliminary study on numerical relativity solutions showed no challenges in testing the no-hair conjecture in the high SNR limit, contrary to the claim presented in [43] and confirming the results presented in [21, 28, 44].

SINGLE KERR MODE

From the spectroscopic analysis the favoured modes are the (3,-3,0), (3,-2,0), (2,1,0) and (2,2,0). A clear mode identification would require the width of the agnostic posterior to overlap with only a single mode, but the statistical uncertainty is too large. The GW150914 inspiral result points to an almost face-off and nearly equal mass BBH, thus the (2,2,0) mode should be the most excited one. Hence, we wondered whether a stronger assumption helps discriminate between the various modes. We run the analysis with a Kerr model:

$$h_+ - ih_\times = \frac{M_f}{D_L} \sum_{lmn} \mathcal{A}_{lmn}\, S_{lmn}(\iota, \varphi)\, e^{i(t - t_{lmn})\tilde{\omega}_{lmn} + \phi_{lmn}},$$
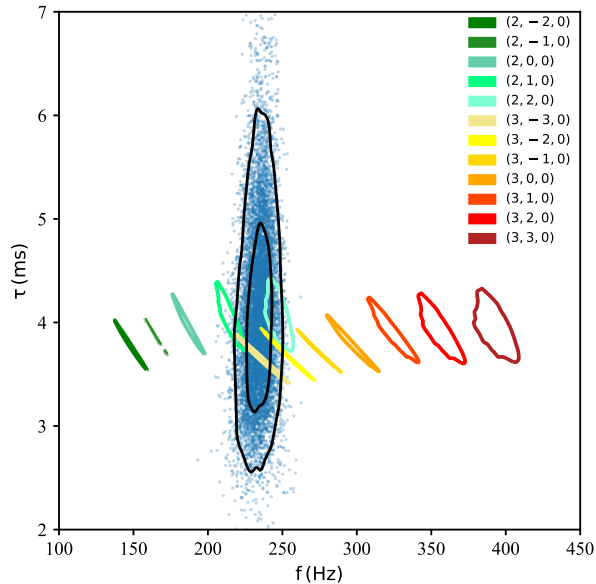
$$(4)$$

FIG. 3. BH spectroscopy from the two- dimensional posterior for central frequency and damping time obtained with a single damped sinusoid ringdown model. The colored contours are the 90% credible intervals for particular (ℓ, m, n) Kerr modes, derived from the LVC reported remnant mass M_f and spin a_f (derived from inspiral). We show the $\ell = 2$ and $\ell = 3$ modes as other ℓ's do not overlap with the posterior distribution.

where $\tilde{\omega}_{lmn} = \omega_{lmn} + i/\tau_{lmn}$ is the complex ringdown frequency determined by the remnant BH mass M_f and its spin a_f. The relations $\omega_{lmn} = \omega_{lmn}(M_f, a_f)$, $\tau_{lmn} = \tau_{lmn}(M_f, a_f)$ follow the formulae given in Ref. [20], available at [39]. S_{lmn} are the spin-weighted spheroidal harmonics [45]. On the other hand, while analytical predictions for the amplitudes $\mathcal{A}_{lmn}$ exist [34, 44, 46, 47] based on the progenitors masses and spins, we do not use them as we wish to estimate them from the data, allowing observational comparisons to the aforementioned theoretical models. Finally, as in the previous analysis, the start time of each mode is left as a free parameter. The prior distribution was uniform for parameters: luminosity distance $D_L \in [10, 1000]$ Mpc, inclination $\cos(\iota) \in [-1, 1]$, $M_f \in [10, 100]$ M$_\odot$, $a_f \in [0, 0.99]$, $\log_{10} A_{lmn} \in [-5, 3]$, $\varphi_i \in [0, 2\pi]$ rad, $t_i \in [3.3, 6.6]$ ms.

In Table I we report, for the most probable modes, the Bayes factors comparing the hypotheses that GW150914 can be described as the ringdown generated by a single given (ℓ, m, n) Kerr mode. Without imposing any restriction on the excitations of the different modes, the given SNR does not allow us to conclusively discriminate between a subset of the $\ell = 2, 3$ modes. The obtained posterior on the sky position parameters and the start time show no appreciable difference with respect to the results already presented in the single damped sinusoid case. The posterior distribution of the orientation parameters $(D_L, \cos(\iota))$ does not show any significant departure
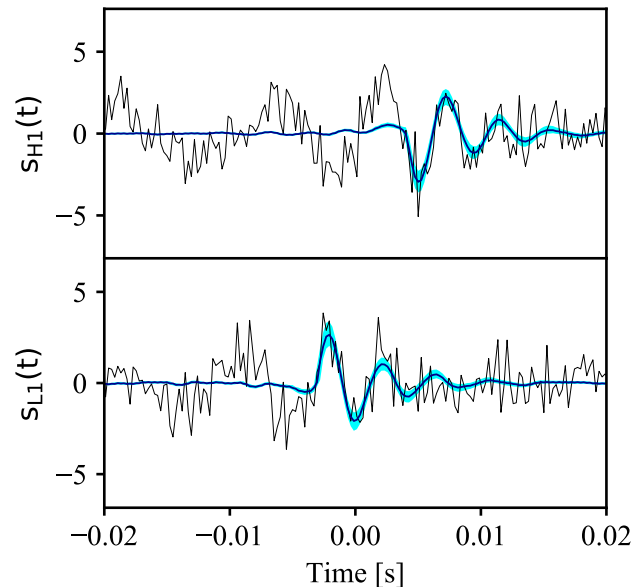

FIG. 4. Reconstructed whitened waveform superimposed on LIGO-Hanford (top panel) and LIGO-Livingston (bottom panel) data. The solid line shows the median recovered waveform, while shaded regions represent 90% credible intervals.

from the prior distribution. This is an indication that, with our model, the event is not loud enough to infer these parameters from the final stage of the coalescence only.

KERR MULTIPLE MODES

Although the unmodelled analysis found no evidence for more than one mode, we repeat the analysis with the Kerr model allowing for the presence of two modes to see whether a more constraining model is able to detect them. Table I reports results for the few combinations that gave the highest Bayes factors. The results on the two Kerr parameters (mass and spin) from this analysis using the $\{(2, 2, 0), (3, -3, 0)\}$ modes is presented in Figure 5. We wish to stress that the posteriors therein do not imply the presence of multiple modes, but rather explain why the Bayes factors indicate that we cannot distinguish between a pure $(2, 2, 0)$, a pure $(3, -3, 0)$ or even a mixture of the two, see Table I. Both modes, in fact, provide similar predictions for central frequency and damping time for GW150914 – see also Fig. 3 – for the typical remnant parameters expected from near-equal mass merging BHs, where $a_f \sim 0.6$ is dominated by the contribution of the orbital angular momentum [48, 49]. From the spectral content only, the inability to discriminate among subsets of modes is thus likely to persist in future ground-based observations. We expect this degeneracy to be lifted either in very loud events or in systems for which the remnant

TABLE I. Summary of the Bayes factors, M_f, a_f median (when measured) and 90% CI obtained with different waveform models (DS stands for Damped Sinusoid) and a transition time prior in $[3.3, 6.6]$ ms. The statistical errors on the log Bayes' factors are ± 0.1. They are estimated computing their variance over 10 different realisations of the pseudo-random number chain initialisation. Within the statistical errors, when differences of $\log B$ are compared against heuristic evidence scales, such as the Jeffreys scale, no significant evidence in favor of any specific mode (or combination of modes) is present.

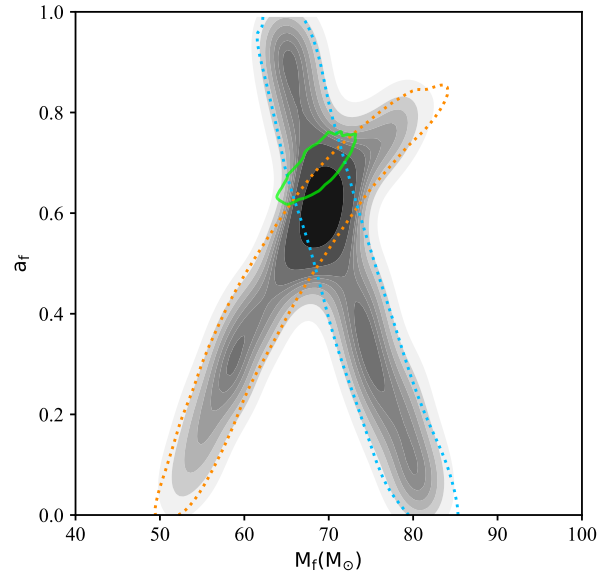| Model	$\log B_{s,n}$	$M_f/M_\odot$	a_f
IMR (LVC)	-	$68.0^{+3.2}_{-3.0}$	$0.69^{0.05}_{0.04}$
DS - 1 mode	56.3	-	-
DS - 2 modes	55.4	-	-
Kerr - $(2,2,0)$ mode	56.5	$64.6^{+14.3}_{-11.4}$	$0.50^{+0.28}_{-0.40}$
Kerr - $(2,1,0)$ mode	56.6	$61.2^{+8.9}_{-8.5}$	$0.60^{+0.28}_{-0.49}$
Kerr - $(2,0,0)$ mode	56.0	$55.0^{+4.1}_{-4.1}$	$0.69^{+0.27}_{-0.58}$
Kerr - $(3,-3,0)$ mode	57.2	$72.3^{+9.7}_{-8.1}$	$0.46^{+0.47}_{-0.42}$
Kerr - $(3,-2,0)$ mode	57.0	$75.7^{+7.1}_{-5.5}$	$0.49^{+0.44}_{-0.43}$
Kerr - $(3,-1,0)$ mode	57.0	$79.9^{+4.5}_{-3.8}$	$0.47^{+0.46}_{-0.43}$
Kerr - $(2,2,0),(3,-3,0)$ modes	56.7	$69.2^{+12.1}_{-14.2}$	$0.50^{+0.40}_{-0.44}$
Kerr - $(2,2,0),(2,1,0)$ modes	56.2	$62.7^{+15.6}_{-9.9}$	$0.54^{+0.31}_{-0.44}$
Kerr - $\ell = 2$ modes	55.0	$55.1^{+15.5}_{-7.9}$	$0.53^{+0.54}_{-0.46}$
Kerr - $\ell = 3$ modes	54.3	$81.9^{+13.2}_{-10.5}$	$0.31^{+0.54}_{-0.28}$
Kerr - $\ell = 2, 3$ modes	52.0	$56.6^{+27.9}_{-10.1}$	$0.39^{+0.47}_{-0.36}$

FIG. 5. Posterior distribution for M_f and a_f assuming the presence of individual modes: $(\ell, m, n) = (2, 2, 0)$ (dotted orange line) or $(\ell, m, n) = (3, -3, 0)$ (blue dotted line), and from a two-modes analysis $\{(2, 2, 0), (3, -3, 0)\}$ whose posterior density is represented in shades of gray. In green, the posterior for M_f and a_f from the LVC IMR analysis. The inferred mass and spin are consistent among the three cases considered, as well as with the LVC posteriors, in line with the Bayes factors, Table I, which indicate no preference towards any of them. See the text for a more in depth explanation.

spin is not dominated by the orbital angular momentum. We also note that, regardless of the final state details, the best systems for spectroscopic studies will be the ones for which the orbital configuration is such that the dominant ringdown mode will be the $(2, -2, 0)$.

Up to now we kept a semi-phenomenological approach, but a more motivated choice of mode combination would be (for example) the use of all m modes for a given ℓ, e.g. for $\ell = 2$ $\{(2, 2, 0), (2, 1, 0), (2, 0, 0), (2, -1, 0), (2, -2, 0)\}$. This more generic model implies a much larger number of parameters to be sampled and, consequently looser bounds. Results for runs using all the $\ell = 2, 3$ modes are summarized in Table I and show no conclusive preference towards one specific ℓ. In all cases, the sky position posterior distribution was found to be completely overlapping with the published LVC result, while D_L and ι cannot be well-estimated due to the complete degeneracy with mode amplitudes. The posterior on start time shows minimal changes with respect to the one obtained by the damped-sinusoid analysis, for all the employed models. Its stability is a strong indication of the robustness of our method, since no variation between different modes start times are expected to be detectable with the SNR contained in the post-merger portion of GW150914.

DISCUSSION

We now focus on a discussion of some of the key assumptions in our analysis. We begin by discussing the effect of varying the lower bound of the prior distribution for the transition time, which earlier we have taken to be uniform in the range $[10, 20]$ M_f after the peaktime of $h_+^2 + h_\times^2$. This choice was guided by numerical relativity studies which looked at the validity of the linearized regime [27, 28, 34], but it is interesting to explore how our inference is affected by relaxing this assumption. We do so by varying the lower bounds of the prior from 0 M_f – corresponding to the peak of the waveform – to 30 M_f in steps of 5 M_f, with prior widths fixed to 10 M_f.

We find that the posterior distribution over t_{start} is dependent on the choice of the prior. For the earliest time prior considered ($t_{start} \in [0.0, 3.3]$ ms, corresponding to $[0, 10]$ M_f), we obtain a measurement of $t_{start} \simeq 1$ ms. For the latest time prior ($t_{start} \in [30, 40]$ M_f), we obtain a flat posterior distribution as the SNR is too small to obtain a measurement. In all other cases, except the more theoretically guided choice ($t_{start} \in [10, 20]$ M_f), we find that the posterior rails against the lower bound of the prior; as noted in [28] the template attempts to be as faithful as possible to the data, while maximising the
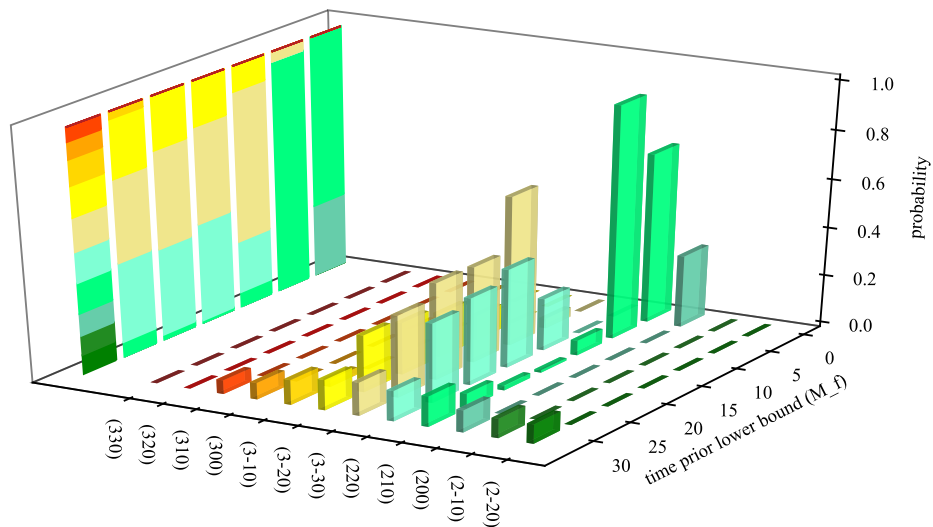
FIG. 6. Mode identification probability as a function of the lower prior bound on the transition time. Each histogram represents the probability that the identified frequency and damping time correspond to the k-th mode as predicted assuming the LVC final mass and spin measurements. The color scheme is the same as in Fig. 3 to ease comparison. As expected, starting the analysis at early times returns frequencies that are lower than that expected for the $(2,2,0)$ mode, and lead to other modes being preferred. In particular, the $(2,1,0)$ mode is the most probable until the start time is smaller than $10\,M_f$ (green histogram). For times between $10\,M_f$ and $25\,M_f$ the most probable modes are the $(2,2,0)$, the $(3,-3,0)$ and the $(3,-2,0)$, aquamarine, khaki and yellow histograms, respectively. Finally, for times greater than $25\,M_f$ the GW150914 signal is too quiet to reliably identify any specific mode. The left most bars summarise the mode probabilities.

recovered signal-to-noise ratio. The sky position recovery is consistent with the result obtained by the LVC [37, 40] when the lower bound of the prior is strictly smaller than $15M_f$. Starting from $15M_f$ onwards, the obtained sky position is biased, reflecting the fact that, at this low SNR, the template tries to latch as early as possible to the data (within the given time prior bounds). The results discussed above are independent of the specific waveform model employed.

The sensitivity to the time prior choice is reflected also in the recovery of the intrinsic parameters of the binary. When using a superposition of damped sinusoids, it will affect mode identification: Fig. 6 shows how the mode identification varies as a function of the time prior. As the lower bound of the time prior approaches the waveform peak, the recovered frequency becomes smaller and smaller due to the waveform latching onto the merger. As consequence, initially, the most probable mode is the $(2,1,0)$ (green histogram). For intermediate times, the situation is the one presented in Fig. 3 where the most probable modes are the $(2,2,0)$, the $(3,-3,0)$ and the $(3,-2,0)$, aquamarine, khaki and yellow histograms, respectively. For start times greater than $25\,M_f$ no inference is possible anymore and all modes become essentially equally probable. In Fig. 7 we show the dependence of the posterior

distribution on the frequency and damping time on the time prior.

When considering a Kerr template[1], Fig. 8 shows how the reconstruction of mass and spin varies as a function of the time prior lower bound. As already discussed, earlier times correspond to smaller recovered frequencies and consequently to larger masses. In all the considered cases the orientation parameter (D_L, ι) posterior distribution shows no departure from its prior distribution, due to the degeneracy with the mode excitation amplitude $\mathcal{A}_n$.

In conclusion, if GR indications on where a ringdown model with a dominant $(2,2,0)$ mode is valid are taken into account to set up a prior on the start time, the recovered parameters of the binary are consistent with the predictions of GR. Moreover a measurement of the effective start time of the ringdown regime can be achieved, excluding both early and late times within the given prior bounds. If later times are allowed by the prior, then the corresponding time posterior rails against its lower bound, signaling a preference towards including the earlier

---

[1] Here we choose the $(2,2,0)$ mode as a representative case, but the considerations presented are common to all the used modes
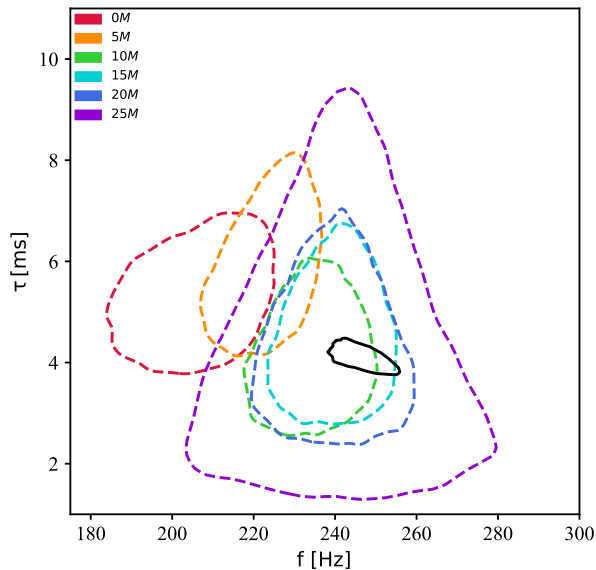
FIG. 7. Effect of the start time prior on the posterior onfthe reconstructed frequency and damping time, when assuming a single damped sinusoid. The solid black band marks the prediction obtained by using the LVC posteriors and assuming the excited mode was the $(\ell, m, n) = (2, 2, 0)$. Using a lower bound on the start time of $30\, M_f$ the obtained reconstruction is flat, thus it is not shown in the plot.

FIG. 8. Effect of the start time prior on the posterior onfthe reconstructed final mass and spin, when assuming a $(\ell, m, n) = (2, 2, 0)$ Kerr mode. The solid black band marks the prediction obtained by using the LVC posteriors. Using a lower bound on the start time of $30\, M_f$ the obtained reconstruction is flat, thus it is not shown in the plot.

portion of the signal in the analysis. If instead the analysis is performed starting from the peak of the waveform, the recovered parameters are biased with respect to the GR prediction, which we interpret as signaling that the system was in a regime where the considered ringdown models do not provide a good description of the emitted radiation. Recent work with NR simulations has suggested that the inclusion of overtones in the model (i.e. $n \neq 0$ modes) allow the ringdown to be extended back toward t_{start} without biasing other parameters [50]. This will be the subject of a subsequent investigation.

SUMMARY

We presented the first comprehensive spectroscopic study of GW150914 ringdown. For the first time, we measured the ringdown onset time from the data, and we found it to be consistent with predictions from numerical relativity. Bayesian model selection indicates that the data do not provide evidence in support of the presence of multiple QNM. We attempted to identify which QNM is dominant, obtaining the (3,-3,0), (3,-2,0), (2,1,0) and (2,2,0) modes as the most probable ones. At the GW150914 SNR, we cannot determine univocally the QNM label, in agreement with preliminary results on numerical relativity waveforms not presented here for brevity. More targeted investigations based on the Kerr
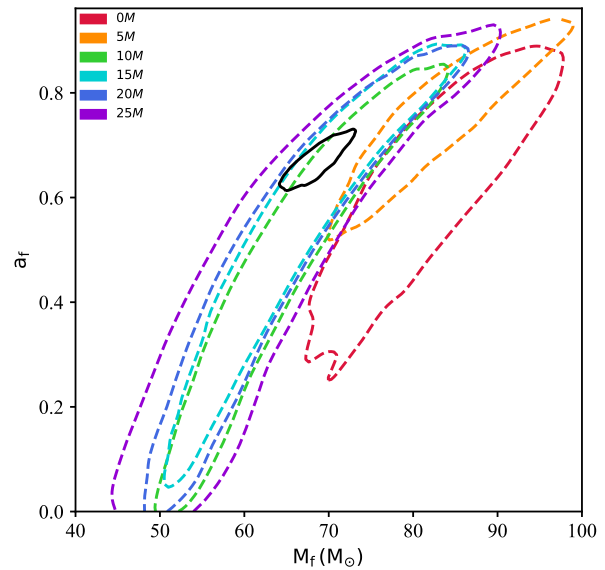
BH solution, confirm our model-independent findings as well as our current lack of mode-resolving power. We note that, due to the similar mode frequencies for the aforementioned subset of modes excited in a near-equal-mass BH coalescences with small spins, BH spectroscopy with a moderate SNR will require the use of information from the inspiral phase to determine the most probable modes. A systematic investigation of the details of our method applied to numerical waveforms, together with the inclusion of refined waveform models incorporating GR numerical predictions, will be presented in a future study. The analysis presented in this paper can and will be applied to louder and/or multiple GW events. Joint coherent analyses will help to test the predictions of linearized GR. Such an extension of the present work will be presented in a future publication. We also defer to a further publication a detailed analysis measuring relative deviations from GR ringdown frequencies [42, 51].

---

[1] B. P. Abbott, R. Abbott, T. D. Abbott, M. R. Abernathy, F. Acernese, K. Ackley, C. Adams, T. Adams, P. Addesso, R. X. Adhikari, et al. (LIGO Scientific Collaboration and Virgo Collaboration), Phys. Rev. Lett. **116**, 061102 (2016), URL https://link.aps.org/doi/10.1103/PhysRevLett.116.061102.

[2] C. V. Vishveshwara, Phys. Rev. D **1**, 2870 (1970), URL https://link.aps.org/doi/10.1103/PhysRevD.1.2870.

[3] W. H. Press, Astrophys. J. **170**, L105 (1971).

[4] S. Chandrasekhar and S. L. Detweiler, Proc. Roy. Soc. Lond. **A344**, 441 (1975).

[5] R. H. Price, Phys. Rev. D **5**, 2439 (1972), URL https://link.aps.org/doi/10.1103/PhysRevD.5.2439.

[6] V. Ginzburg and L. Ozernoy, Zh. Eksp. Teor. Fiz. **147**, 1030 (1964).

[7] A. Doroshkevic, Y. B. Zeldovich, and I. Novikov, Sov. Phys. JETP 36 1 (7) (1965).

[8] W. Israel, Phys. Rev. **164**, 1776 (1967), URL https://link.aps.org/doi/10.1103/PhysRev.164.1776.

[9] B. Carter, Phys. Rev. Lett. **26**, 331 (1971), URL https://link.aps.org/doi/10.1103/PhysRevLett.26.331.

[10] S. W. Hawking, Communications in Mathematical Physics **25**, 152 (1972), ISSN 1432-0916, URL https://doi.org/10.1007/BF01877517.

[11] D. C. Robinson, Phys. Rev. Lett. **34**, 905 (1975), URL https://link.aps.org/doi/10.1103/PhysRevLett.34.905.

[12] P. O. Mazur, J. Phys. **A15**, 3173 (1982).

[13] G. Bunting, Ph. D. Thesis (unpublished) University of New England, Armidale, N. S. W. (1983).

[14] F. Pretorius, *Gravitational wave observation of dynamical, strong-field gravity*, Stephen Hawking 75th Birthday Conference on Gravity and Black Holes, DAMTP, Cambridge (2017).

[15] M. Dafermos and I. Rodnianski, Clay Math. Proc. **17**, 97 (2013), 0811.0354.

[16] V. Cardoso, E. Franzin, and P. Pani, Phys. Rev. Lett. **116**, 171101 (2016), URL https://link.aps.org/doi/10.1103/PhysRevLett.116.171101.

[17] S. Hod, Phys. Rev. **D84**, 124030 (2011), 1112.3286.

[18] G. Raposo, P. Pani, and R. Emparan (2018), 1812.07615.

[19] O. Dreyer, B. J. Kelly, B. Krishnan, L. S. Finn, D. Garrison, and R. Lopez-Aleman, Class. Quant. Grav. **21**, 787 (2004), gr-qc/0309007.

[20] E. Berti, V. Cardoso, and C. M. Will, Phys. Rev. **D73**, 064030 (2006), gr-qc/0512160.

[21] R. Brito, A. Buonanno, and V. Raymond, Phys. Rev. **D98**, 084038 (2018), 1805.00293.

[22] H. Yang, K. Yagi, J. Blackman, L. Lehner, V. Paschalidis, F. Pretorius, and N. Yunes, Phys. Rev. Lett. **118**, 161101 (2017), 1701.05808.

[23] B. P. Abbott, R. Abbott, T. D. Abbott, M. R. Abernathy, F. Acernese, K. Ackley, C. Adams, T. Adams, P. Addesso, R. X. Adhikari, et al. (LIGO Scientific and Virgo Collaborations), Phys. Rev. Lett. **116**, 221101 (2016), URL https://link.aps.org/doi/10.1103/PhysRevLett.116.221101.

[24] B. P. Abbott et al. (VIRGO, LIGO Scientific) (2013), [Living Rev. Rel.19,1(2016)], 1304.0670.

[25] J. Aasi et al. (LIGO Scientific), Class. Quant. Grav. **32**, 074001 (2015), 1411.4547.

[26] F. Acernese et al. (Virgo), Class. Quant. Grav. **32**, 024001 (2015), 1408.3978.

[27] S. Bhagwat, M. Okounkova, S. W. Ballmer, D. A. Brown, M. Giesler, M. A. Scheel, and S. A. Teukolsky, Phys. Rev. **D97**, 104065 (2018), 1711.00926.

[28] G. Carullo et al., Phys. Rev. **D98**, 104020 (2018), 1805.04760.

[29] M. Cabero, C. D. Capano, O. Fischer-Birnholtz, B. Krishnan, A. B. Nielsen, A. H. Nitz, and C. M. Biwer, Phys. Rev. **D97**, 124069 (2018), 1711.09073.

[30] R. P. Kerr, Phys. Rev. Lett. **11**, 237 (1963).

[31] *The gravitational-wave open science center*, URL https://www.gw-openscience.org/about/.

[32] M. Vallisneri, J. Kanner, R. Williams, A. Weinstein, and B. Stephens, J. Phys. Conf. Ser. **610**, 012021 (2015), 1410.4839.

[33] W. Del Pozzo and J. Veitch, *CPNest: an efficient python parallelizable nested sampling algorithm*, https://github.com/johnveitch/cpnest.

[34] L. London, D. Shoemaker, and J. Healy, Phys. Rev. D **90**, 124032 (2014), URL https://link.aps.org/doi/10.1103/PhysRevD.90.124032.

[35] T. D. Abbott et al. (LIGO Scientific, Virgo), Phys. Rev. **X6**, 041014 (2016), 1606.01210.

[36] W. G. Anderson, P. R. Brady, J. D. Creighton, and É. É. Flanagan, Phys. Rev. D **63**, 042003 (2001), gr-qc/0008066.

[37] https://dcc.ligo.org/LIGO-T1800235/public.

[38] X. Jiménez-Forteza, D. Keitel, S. Husa, M. Hannam, S. Khan, and M. Pürrer, Phys. Rev. D **95**, 064024 (2017), URL https://link.aps.org/doi/10.1103/PhysRevD.95.064024.

[39] https://pages.jh.edu/~eberti2/ringdown/.

[40] B. P. Abbott et al. (Virgo, LIGO Scientific), Phys. Rev. Lett. **116**, 241102 (2016), 1602.03840.

[41] W. Del Pozzo, C. P. Berry, A. Ghosh, T. S. F. Haines, L. P. Singer, and A. Vecchio, Mon. Not. Roy. Astron. Soc. **479**, 601 (2018), 1801.08009.

[42] S. Gossan, J. Veitch, and B. S. Sathyaprakash, Phys. Rev. D **85**, 124056 (2012), URL https://link.aps.org/doi/10.1103/PhysRevD.85.124056.

[43] E. Thrane, P. D. Lasky, and Y. Levin, Phys. Rev. **D96**, 102004 (2017), 1706.05152.

[44] V. Baibhav, E. Berti, V. Cardoso, and G. Khanna, Phys. Rev. **D97**, 044048 (2018), 1710.02156.

[45] E. Berti and A. Klein, Phys. Rev. **D90**, 064012 (2014), 1408.1860.

[46] I. Kamaretsos, M. Hannam, S. Husa, and B. S. Sathyaprakash, Phys. Rev. D **85**, 024018 (2012), URL https://link.aps.org/doi/10.1103/PhysRevD.85.024018.

[47] L. T. London (2018), 1801.08208.

[48] A. Buonanno, L. E. Kidder, and L. Lehner, Phys. Rev. D **77**, 026004 (2008), URL https://link.aps.org/doi/10.1103/PhysRevD.77.026004.

[49] J. G. Baker, W. D. Boggs, J. Centrella, B. J. Kelly, S. T. McWilliams, and J. R. van Meter (2008), arXiv:0805.1428.

[50] M. Giesler, M. Isi, M. Scheel, and S. Teukolsky (2019), 1903.08284.

[51] J. Meidam, M. Agathos, C. Van Den Broeck, J. Veitch, and B. S. Sathyaprakash, Phys. Rev. D **90**, 064009 (2014), URL https://link.aps.org/doi/10.1103/PhysRevD.90.064009.